AIAA 2001-2210

Rotor Broadband Noise Prediction with Comparison to Model Data

Thomas F. Brooks and Casey L. Burley
NASA Langley Research Center
Hampton, VA 23681-2199

7th AIAA/CEAS
Aeroacoustics Conference
May 28-30, 2001 / Maastricht, The Netherlands

AIAA-2001-2210

Rotor Broadband Noise Prediction with Comparison to Model Data

Thomas F. Brooks*
Casey L. Burley†

NASA Langley Research Center
Hampton, Virginia 23681-2199

ABSTRACT

This paper reports an analysis and prediction development of rotor broadband noise. The two primary components of this noise are Blade-Wake Interaction (BWI) noise, due to the blades' interaction with the turbulent wakes of the preceding blades, and "Self" noise, due to the development and shedding of turbulence within the blades' boundary layers. Emphasized in this report is the new code development for Self noise. The analysis and validation employs data from the HART program, a model BO-105 rotor wind tunnel test conducted in the German-Dutch Wind Tunnel (DNW). The BWI noise predictions are based on measured pressure response coherence functions using cross-spectral methods. The Self noise predictions are based on previously reported semi-empirical modeling of Self noise obtained from isolated airfoil sections and the use of CAMRAD.Mod1 to define rotor performance and local blade segment flow conditions. Both BWI and Self noise from individual blade segments are Doppler shifted and summed at the observer positions. Prediction comparisons with measurements show good agreement for a range of rotor operating conditions from climb to steep descent. The broadband noise predictions, along with those of harmonic and impulsive Blade-Vortex Interaction (BVI) noise predictions, demonstrate a significant advance in predictive capability for main rotor noise.

SYMBOLS

BTE	blunt trailing edge
BVI	blade vortex interaction
BWI	blade wake interaction
C	rotor blade chord
C_T	rotor thrust coefficient, thrust / $\rho_0 \pi R^2 (\Omega R)^2$
c_0	medium speed of sound
$\overline{D}_h$	high-frequency directivity function
$\overline{D}_l$	low-frequency directivity function
f	frequency at observer with a common bandwidth of $(\Delta f)_T$, Hz
f	frequency with respect to blade segment
f_0	frequency (Doppler shifted) with respect to observer
G	autospectrum of acoustic or unsteady surface pressure
H	grouping of amplitude and shape functions defined in Ref. 27
LBL-VS	laminar boundary layer - vortex shedding
LE	leading edge
L	blade segment width (spanwise)
M	Mach number, U/c_0
R	rotor radius
Re_c	Reynolds number based on C and U
r	radial distance from hub
r	distance from observer from a coordinate system centered on blade segment
SPL	sound pressure level, dB (re 2×10^{-5} Pa)
TBL-TE	turbulent boundary layer - trailing edge
TE	trailing edge
t_r	propagation time to observer
U	flow speed normal to span (U_{mn} with mn suppressed)
V_{mn}	translation speed of mn^{th} blade segment, $\lvert\mathbf{V}_{mn}\rvert$
V_{wt}	wind tunnel air speed, $\lvert\mathbf{V}_{wt}\rvert$
$\mathbf{V}$	velocity vector
$\mathbf{X}$, $\mathbf{X}'$	(x,y,z) and (x',y',z') coordinate systems / observer locations, see Figs. 10,11, and 12
$\mathbf{X}_e$	(x_e, y_e, z_e) coordinate system centered at TE of blade segment
$\mathbf{X}_T$	(x_T, y_T, z_T) tunnel coordinates centered at rotor hub

*Senior Research Scientist, Aeroacoustics Branch, Associate Fellow AIAA.

†Senior Research Scientist, Aeroacoustics Branch

α	rotor tip-path-plane angle referenced to tunnel streamwise axis, positive for backward tilt
α_*	blade segment angle of attack to U
α_p	blade segment pitch angle with respect to rotor disk
β	Glauert-Prandtl compressibility factor, $(1-M^2)^{-1/2}$
δ	boundary layer thickness
δ^*	boundary layer displacement thickness
μ	advance ratio, $V_{wt}/\Omega R$
ρ_0	freestream air density
Ω	rotor rotation frequency, rad/sec or rpm
ω	circular frequency, rad/sec
Ψ	rotor azimuth angle

subscripts

cor	corrected
ind	induced rotor flow
m	index of blade segment spanwise location
n	index of blade segment azimuth location
p	pressure side of blade segment
r	retarded
s	suction side of blade segment
T	rotor period, rev/s
tot	total
wt	wind tunnel

INTRODUCTION

Over the last several decades, helicopter noise, and to a lesser extent tiltrotor noise, has been intensely studied. The emphasis has been on the measurement and prediction of harmonic and impulsive noise - related to rotor blade thickness and loading effects. A good example of predictive capability is that of CAMRAD.Mod1/HIRES[1]. These are aeroacoustic codes for rotor harmonic and BVI noise, which has evolved to become the key elements of a system noise prediction capability called TRAC, for Tilt Rotor Aeroacoustic Codes[2]. These codes have been used over the last several years to successfully examine and explain helicopter windtunnel[1] and flight[3] results, as well as tiltrotor windtunnel[2,4] and flight[5,6] test results. Absent in the predictions, however, are the important broadband noise portions of the main rotor spectra. For the flight tests examined, significant portions of the measured noise spectra in the mid to higher frequency ranges were substantially under-predicted. The vehicles did not have tail rotors to contribute noise in this frequency range. (The helicopter test[3] involved the MD 900, which is a NOTAR (NO TAil Rotor) vehicle, and the tiltrotor tests[5,6] were of the XV-15 vehicle.) It comes as no surprise that the higher frequency ranges are often controlled by main rotor broadband noise, rather than harmonic and impulsive noise. A main rotor broadband noise study[7] in the mid-1980's was the first to identify mid-frequency Blade-Wake Interaction (BWI) noise source, which is due to blade interaction with turbulence encountered within the wake of previous blades. For years previously, this mid-frequency noise was thought to be due to rotor ingestion of naturally occurring atmospheric turbulence. This study also demonstrated the importance of high frequency broadband "Self" noise, which is noise related to the formation and shedding of self-induced boundary layer turbulence. The importance of these sources in terms of the standard noise annoyance metric dBA was demonstrated in a follow-up analysis[8] of the BO-105 model data[7], when scaled to that of a full-size rotor. While BVI noise was found to dominate dBA in descent and level flight conditions, the BWI noise dominated in level flight to mild climb conditions, and Self noise dominated during mild to steep climb conditions.

Figure 1 illustrates these flow characteristics responsible for the BVI, BWI, and Self noise. A blade is shown encountering a flow field containing tip vortices (represented by the vortex tubes) surrounded by their associated rolled-up wake turbulence and the turbulence surrounding the 'rotor-disk vortex' and the inboard wake. Turbulence is also shown over the surface within the boundary layer and near-wake. Impulsive BVI noise is produced by the blade's interaction with the tip or inboard-originated vortices that are of predetermined positions with respect to any blade position. This allows a deterministic solution to the BVI blade loading and thus BVI noise at harmonics of the blade passage frequency. The flow details of the turbulence in the wake and within the boundary layers are non-deterministic and thus approached analytically in a statistical wave-number or spectral fashion. BWI noise is produced by the blade's leading edge loading response to the turbulence encounters. The Self noise is predominately trailing edge noise due to the scattering of the turbulence pressure field from the passage of turbulence over the trailing edge into the near-wake.

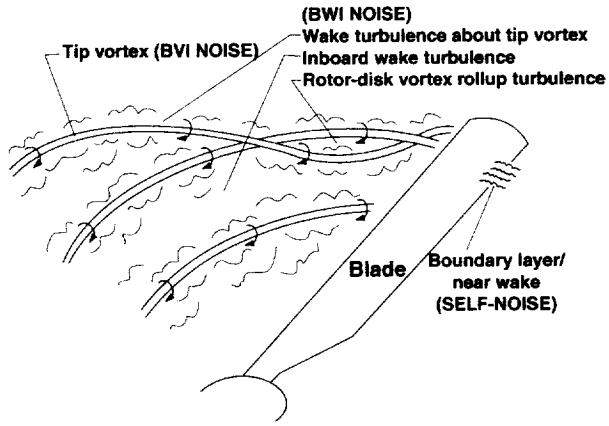

Figure 1. Flow field encountered by a rotor blade.

In this paper, we briefly review the status of the Langley prediction codes that are pertinent for the present study. Self noise prediction and its historical background is emphasized, as harmonic, BVI, and BWI noise prediction methods are presented elsewhere. In the succeeding sections, analysis is given on data obtained during an extensive aeroacoustic model rotor windtunnel study called HART. Acoustic pressure time histories and spectra are used to illustrate the character of the noise sources. A high-frequency integrated noise metric is defined and contour plotted to show Self noise directivity over a plane under the rotor for conditions ranging from climb to steep descent. The implementation of the Self noise prediction model is described. Predictions are then compared with measured data.

AEROACOUSTIC PREDICTION

Pertinent aeroacoustic prediction codes for the present study are highlighted in Fig. 2. The harmonic and impulsive noise prediction codes are a subset of the TiltRotor Aeroacoustic Codes (TRAC) at NASA Langley. The Broadband Acoustic Rotor Codes (BARC) designates combined coding for BWI noise and Self noise predictions.

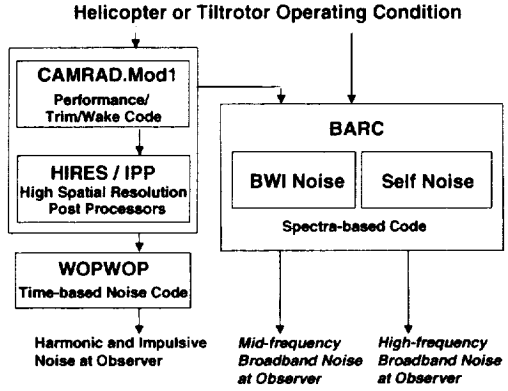

Figure 2. Prediction code elements.

Harmonic and BVI noise

The development of the harmonic and impulsive BVI noise codes is presented in Ref. 1. The three components are: CAMRAD.Mod1 -- a substantially modified version of the performance/trim/wake code CAMRAD[9]; HIRES/IPP -- a high-resolution blade loads post-processor; and WOPWOP[10] -- an acoustic code. The added features in CAMRAD.Mod1, compared to CAMRAD, enhance the aerodynamic, wake, and dynamic modeling in a way that is important for noise prediction. One such feature is vortex/wake modeling that more accurately reflects the relationship between the blade loading details and the wake structure, strength, and position. HIRES is a high-spatial-resolution extension to CAMRAD.Mod1. IPP is an Indicial Post Processor that employs the Beddoes[11,12] indicial aerodynamic blade-response modeling to determine the high-resolution compact loading for the time-based rotor acoustic prediction code WOPWOP, which implements the acoustic formulation 1A of Farassat[13]. The success of these codes was demonstrated in Ref. 1 and other studies indicated previously.

BWI noise

Brooks, et al[7,8] showed that mid-frequency main rotor broadband noise is due to Blade Wake Interaction. Following this, Glegg[14] developed a prediction model that related the radiated sound to the spectrum of the postulated turbulence encountered by the blades. The turbulence was modeled as being positioned uniformly around tip vortices. The acoustic field was calculated from the unsteady loads on the blades, which were estimated from the blade response function of Amiet[15] for unsteady upwash gusts. Glegg[16] refined the prediction method by basing the turbulence description inputs on the measurements of Wittmer, et al[17,18,19]. The noise predictions improved in spectral shape but tended to under-predict the overall levels compared to the measurements[7].

Burley, et al[20] bypassed the uncertainty in the turbulence description by employing measured blade response to the wake turbulence in noise prediction modeling. The study defined the radial and azimuthal distribution of the BWI noise source in a quantitative manner and utilized this for prediction. The extensive aeroacoustic database from the HART test (to be discussed) was used. Blade response coherence functions were determined using cross-correlation methods between surface pressure sensors. These were used in a noise radiation formulation of Amiet[15]. Radiation to an observer from individual blade segments accounted for Doppler and convective amplification effects. The predictions found very good directivity and spectral agreement with measured noise for a large range of rotor flight conditions. It is noted that Brezillon, et al.[21] also analyzed experimental acoustic and unsteady blade surface pressures from the HART test along with rotor wake simulations. Directivity and spectra of BWI and BVI noise were compared for several flight conditions. Although no prediction method was proposed, the basic characteristics and importance of BWI were confirmed.

The method of Burley, et al.[20] is the BWI noise prediction method of BARC in Fig. 2. A present limitation of this method is that measured blade loading is required for noise prediction. To generalize the method, further measurement and modeling of rotor wake turbulence and blade response are required.

Self noise

Besides showing the importance of Self noise in the rotor spectrum, Brooks, et al[7] demonstrated that prediction of rotor Self noise is feasible by utilizing noise results from isolated non-rotating blade segment tests. These tests were a series of Self noise and aerodynamic experiments by Brooks, et al[22-26] using two- and three-dimensional NACA 0012 airfoil sections subjected to uniform flow in an anechoic flow facility. A large range of chordlengths from 1 to 24 inches, angles of attack from 0° to 25.2°, and source diagnostics were examined. The Reynolds number ranged up to Re_c=3 x 10^6 based on chord and Mach number up to M = .21. Analysis revealed the apparent existence of multiple Self noise mechanisms, and scaling laws of each were developed based on the data and fundamental aeroacoustic theory. A report by Brooks, et al.[27] documented the basic scaling laws and prediction developments. The predictions included successful comparisons with published data from three different Self noise studies (Schlinker, et al[28,29,30]) of different airfoil shapes, which were tested up to M and Re_c values of .5 and 4.6×10^6, respectively. Figure 3 illustrates the blade section flow characteristics leading to specific scaling models of Ref. 27.

The total Self noise spectrum $G_{Self}(f)$ at an observer is the sum of noise spectra contributions of the individual sources. In present terminology:

$$G_{Self}(f) = G_{TBL-TE}(f) + G_{LBL-VS}(f) + G_{BTE}(f) + G_{Tip}(f) \quad (1)$$

Here, $G_{TBL-TE}(f)$ represents *Turbulent Boundary Layer - Trailing Edge* (TBL-TE) noise, due to pressure scattering from the passage of turbulence over the TE into the near-wake. It contains contributions from the pressure side of the blade segment, $G_{TBL-TE,p}(f)$ and from the suction side, $G_{TBL-TE,s}(f)$, as well the TE separated flow noise $G_{TBL-TE,\alpha_*}(f)$, which occurs at angles of attack $|\alpha_*| > 0°$.

$$G_{TBL-TE}(f) = G_{TBL-TE,p}(f) + G_{TBL-TE,s}(f) + G_{TBL-TE,\alpha_*}(f) \quad (2)$$

where

$$G_{TBL-TE,p}(f) = \frac{\delta_p^* M^5 L \bar{D}_h}{r_e^2} \cdot H_p\left(\frac{f\delta_p^*}{U}, M, Re_c, Re_{\delta_p^*}\right), \quad (3)$$

$$G_{TBL-TE,s}(f) = \frac{\delta_s^* M^5 L \bar{D}_h}{r_e^2} \cdot H_s\left(\frac{f\delta_s^*}{U}, M, Re_c\right), \quad (4)$$

and

$$G_{TBL-TE,\alpha_*}(f) = \frac{\delta_s^* M^5 L \bar{D}_h}{r_e^2} \cdot H_{\alpha_*}\left(\frac{f\delta_s^*}{U}, \alpha_*, M, Re_c\right). \quad (5)$$

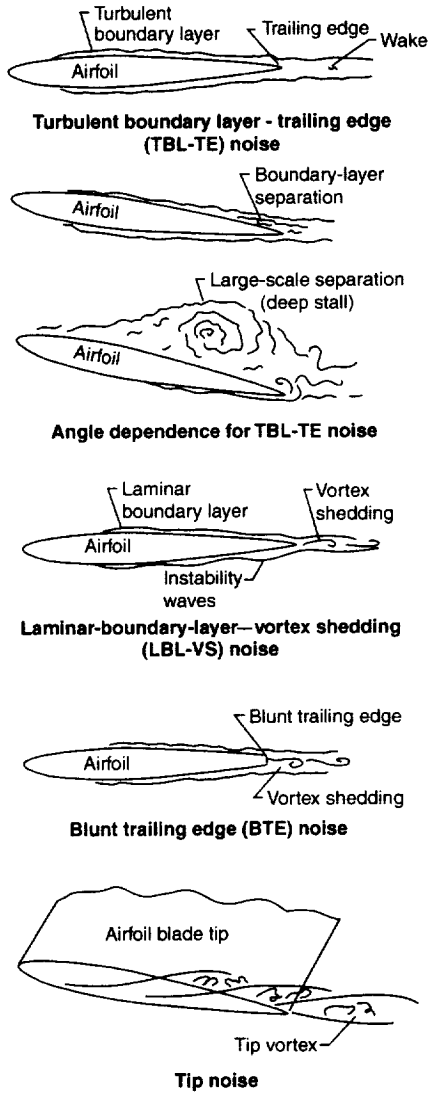

Figure 3. Illustration of flow conditions producing blade Self noise.

When α_* becomes larger than a value dependent on M and Re_c, or $|\alpha_*| > 12.5°$, whichever is first, stall occurs and

$$G_{TBL-TE,p}(f) = 0 \quad (6)$$

$$G_{TBL-TE,s}(f) = 0 \quad (7)$$

and

$$G_{TBL-TE,\alpha_*}(f) = \frac{\delta_s^* M^5 L \bar{D}_l}{r_e^2} \cdot H'_{\alpha_*}\left(\frac{f\delta_s^*}{U}, \alpha_*, M, Re_c\right) \quad (8)$$

In the above equations, the first grouping of terms on the right hand side reflects the fact that the basic scaling approach is that of Ffowcs Williams and Hall[31] - for the

problem of turbulence passing the trailing edge of an extended half-plane surface. The boundary layer displacement thicknesses δ_p^* and δ_s^* for the pressure and suction sides, respectively, represent length scales. The Mach number, $M = U/c_0$, represents that component of velocity U normal to the span, and L is the blade-segment spanwise length. The half-plane-baffled-type directivity term $\overline{D}_h$ for higher frequency trailing edge noise and the dipole directivity term $\overline{D}_l$ for lower frequency stall noise, are presented in a following section addressing the coordinate system of the rotor. The observer distance in retarded coordinates from the TE is r_e. The terms H_p, H_s, H_{α_*}, and H'_{α_*} represent groupings of amplitude and spectral shape functions that are defined in Ref. 27. It is noted that the boundary layer displacement thicknesses on the two sides, as well as boundary layer thicknesses, δ_p and δ_s, to be used below, are computed as functions[27] of Re_c and α_* which were derived from detailed near-wake flow measurements from the aforementioned isolated NACA 0012 blade section studies.

Laminar Boundary Layer - Vortex Shedding (LBL-VS) noise contributes at conditions conducive to laminar boundary layer flow on at least one side of the blade. The noise is generally multi-tonal in character but contributes broadly over the frequency range. It is scaled in a broadband manner (using a one-third Octave resolution) similar to that used for TBL-TE noise. This noise contribution is

$$G_{LBL-VS}(f) = \frac{\delta_p M^5 L \overline{D}_h}{r_e^2} \cdot H_l\left(\frac{f\delta_p}{U}, \alpha_*, M, \mathrm{Re}_c\right) \qquad (9)$$

where δ_p is the boundary layer thickness and H_l is an amplitude and spectral shape function[27].

Blunt Trailing Edge (BTE) noise is due to vortex shedding from a less-than-sharp trailing edge. The noise contribution is

$$G_{BTE}(f) = \frac{hM^{5.5} L \overline{D}_h}{r_e^2} \cdot H_b\left(\frac{h}{\delta^*_{avg}}, \frac{f\delta^*_{avg}}{U}, \frac{fh}{U}, \psi\right) \qquad (10)$$

where h is the trailing edge thickness and δ^*_{avg} is the average boundary layer displacement thickness of the pressure and suction sides at the TE. The angle ψ is the solid angle between the blade surfaces immediately upstream of the TE. The amplitude and shape function H_b reveals the mechanism is most intense and most tonal in spectral shape for large h/δ^*_{avg} and small ψ.[27]

Tip noise is due to the formation and shedding of the tip vortex. It is modeled as TE noise due to the passage of turbulence, formed within the tip vortex, over the TE. This noise contribution is

$$G_{Tip}(f) = \frac{M^2 M_{\max}^3 \ell \overline{D}_h}{r_e^2} \cdot H_t\left(\frac{f\ell}{U}, \alpha'_{Tip}\right) \qquad (11)$$

where $M_{\max}$ is the maximum velocity in or about the vortex near the TE, which is a function of M and an effective blade angle α'_{Tip} at the blade tip. The spanwise extent of the vortex formation at the TE is ℓ which is a function of chordlength C and α'_{Tip}. Different definitions for ℓ are given for rounded and flat edge tips.[27]

Use of Self noise code[27] in previous rotary blade studies – In Brooks, et al[7], the above Self noise equations were used to predict broadband noise for a BO-105 model main-rotor broadband noise test. Rotor definition and flight conditions, specified as thrust, rotor angle, rotor speed, advance ratio, and trim conditions (zero rotor flapping) were provided as input into the ROTONET[32] rotor performance module. The module assumed a fully articulated rotor with rigid blades and a simple uniform inflow model. (Such modeling is considered simplistic compared to present day rotor modeling such as in CAMRAD.Mod1.) The module determined local blade segment velocities and angles of attack for a number of azimuthal positions. The source strengths for each blade segment were calculated, based on a pseudo-steady assumption for boundary layer conditions, and the ROTONET noise radiation module was used to sum contributions from all blade segments to obtain the total predicted Self noise spectrum at the observer. The predictions were limited to a single observer directly above the rotor center and out of the flow, so neither Doppler, convective, nor directivity effects were examined. The predictions produced good qualitative and, for many cases, good quantitative comparisons with the measured data. Appendix C of Ref. 27 suggested code-running improvements for those cases.

The Self noise code[27] has found substantial use in wind turbine noise prediction applications - particularly in Europe, as indicated in an extensive review by Wagner, et al[33]. Dunbabin, as cited by Wagner, et al., implemented the code and extended it with a model for inflow of atmospheric turbulence. Lowson[34,35,36,37] used the data of Ref. 27 to perform a re-analysis, which produced different noise models that required less input for the wind turbine application. Pettersson[38] implemented the code[27] with a modification that allowed the consideration of serrated edges. Bareiss, et al.[39] examined modified blade tips. It was found for different tips that the code[27] predictions are best when applying actual wind turbine boundary layer data. Lowson[36] performed a systematic comparison of a number of sets of spectral data from modern wind turbines and found that overall levels can be predicted within several dB. However, many of the details of the spectral shape were not reproduced by several codes.

Glegg[40,41] used the Self noise code as a basis for a broadband Self noise prediction from ducted fans. Strip theory and radially-dependent flow conditions were used as input to predict noise from rotating cascaded blades. A method was introduced for coupling the modes in a circular duct to the modes of a linear cascade. For noise strength definition, Glegg used a theoretical approach of Amiet[42] to relate radiated noise to boundary layer pressure fluctuations on blade surfaces. Noise prediction equations[27] were used in an inverted manner to obtain the locally defined pressure spectra and correlation lengths. Comparisons[41] of theory with model fan data showed correct noise trends with fan loading, but a tended to over-predict at high fan speeds, where the blade tip speed is transonic.

TEST DESCRIPTION

The data employed in this paper is that of an international cooperative rotor noise research study by researchers from the US Army Aeroflightdynamics Directorate (AFDD), NASA Langley, the German-Dutch Wind Tunnel (DNW), and the Aerospace Research Establishments of France (ONERA) and Germany (DLR). The HART[43] (Higher-harmonic control Aeroacoustic Rotor Test) program was conducted in 1994 in the German-Dutch Wind Tunnel (DNW). Details of the test program and major results are reported by Splettstoesser, et al[44] and Kube et al[45].

In Fig. 4, the DLR rotor model test stand is shown mounted on a sting in the DNW anechoic open test section. The open-jet configuration employed an 8m wide by 6m height nozzle, which provided a 1.9m long free jet with a low-turbulence potential core. The traversing in-flow microphone array is seen located underneath the rotor hub. The test stand fuselage, sting and traverse were acoustically treated to minimize reflections. The rotor hub was positioned 7m downstream of the nozzle and 1m above the tunnel center. The rotor is a 40-percent dynamically and Mach scaled model of the BO-105 hingeless main rotor. It is four-bladed, 4m in diameter and has a pre-coning of 2.5^0 at the hub. The blades are rectangular in planform, have a chordlength of .121m, NACA 23012 sections, -8^0 linear twist and standard rectangular tips. The rotor operated in the counter clockwise direction with a nominal rotor operational speed of 1040 rpm, which results in an acoustic blade passage frequency (bpf) of about 70 Hz. For all rotor conditions reported here, the nominal hover tip Mach number is .641, rotor C_T= .0044, μ = .15 and the hub lateral and longitudinal moments were trimmed to be nominally zero. The flapping angles were nominally zero – hence, for this study, shaft angle is equivalent to tip-path-plane angle.

The blades were highly instrumented with unsteady surface pressure transducers. The transducer results were used extensively for BVI and harmonic loading studies[44] and BWI studies[20], but not in this study for Self noise because of placement and high frequency response limitations.

The rotor noise field was measured by eleven microphones mounted on the traverse located 2.3m below the rotor, as shown in Figure 4. The eleven microphones were arranged symmetrically with respect to the tunnel centerline and equally spaced .54m apart. Acoustic data were acquired at streamwise locations that were .5m apart over a large plane below the rotor generally ranging from 4m upstream to 4m downstream of the rotor center. The resulting measurement grid plane is shown in Fig. 5. The rotor disk edge is projected down to the plane to better show relative microphone positions. The microphones were 1/2-inch pressure-type condenser microphones (B&K 4134). Small frequency-dependent amplitude corrections were made to the data to account for the presence of "bullet" nose cones, per manufacturer's nominal calibrations. The acoustic data were sampled at a rate of 2048/rev over a period of 30 rotor revolutions. The useful frequency ranged up to approximately 16 kHz. The acoustic samples were acquired whenever the rotor blades were at the same azimuthal position for every rotor revolution sampled. The background noise levels were found to be low (as subsequently shown), thus resulting in good signal-to-noise ratio for the measured rotor noise.

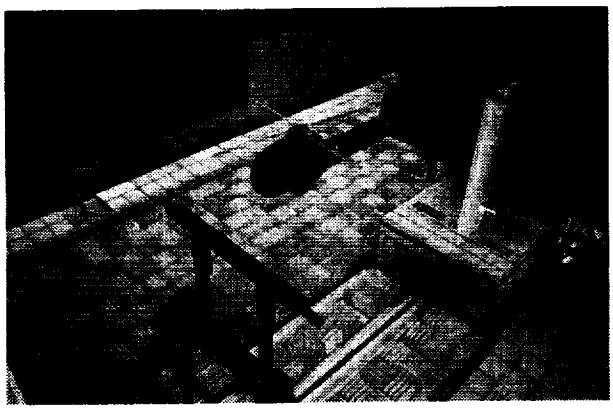

Figure 4. The BO-105 model rotor and in-flow microphone traverse in the DNW open test section.

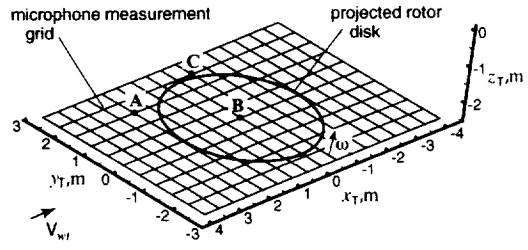

Figure 5. Microphone measurement plane below the rotor disk. Orientation is same as Fig. 4.

TEST RESULTS

Character of Noise Sources

Acoustic pressure signatures for a descent rotor test condition are shown in Fig. 6 for microphone positions, A and B of Fig. 5. Fig. 6(a) shows two sample time histories (samples 10 and 15), for the upstream (forward) microphone A under the rotor's advancing side. The instantaneous as well as the average (over 30 samples) time histories show a strong impulsive BVI character. The time histories obtained by subtracting the average from each instantaneous sample represent the non-deterministic portion of the noise for each sample. Unsteady BVI noise, as well as BWI and Self broadband noise, is labeled in the figure. The BVI unsteadiness is termed "jitter" by Brooks[46], who shows this causes energy smearing of the BVI noise spectra. The BWI and Self noise portion of the time histories is of higher frequency than the unsteady BVI and appears most concentrated in "patches" about the BVI. The last two time histories shown in Fig. 6(a) are the instantaneous minus the average signals that are band-passed filtered from 10 to 16 kHz. (Note the reduced amplitude scale on the time histories.) As will be seen in spectral presentations to follow, this filtering accentuates the Self noise portion of the signal, leaving only some residual unsteady BVI and BWI. The Self

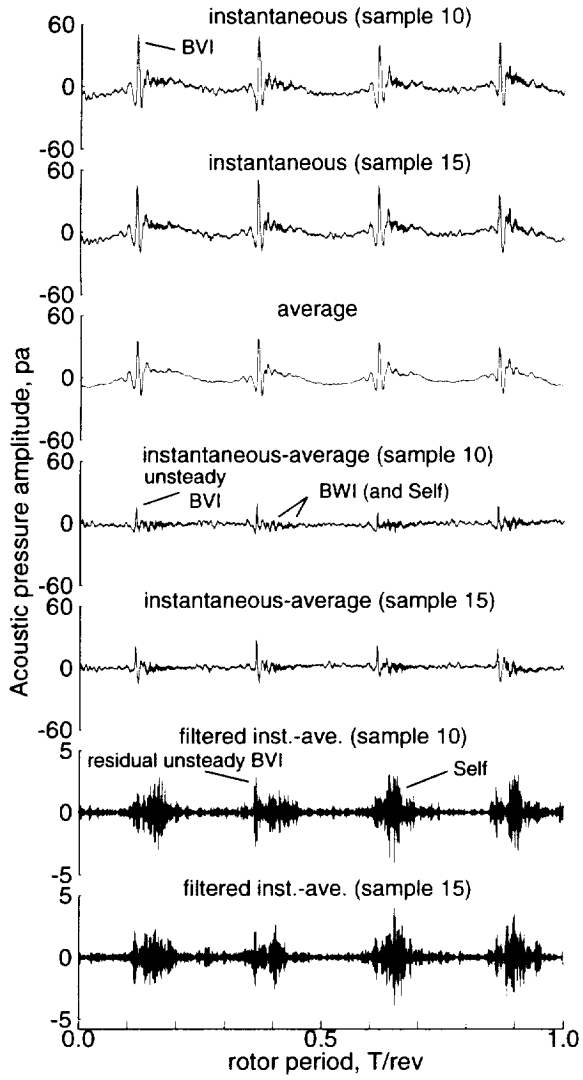

(a) Microphone location A upstream under the advancing side (x_T=2.0m,y_T=1.6m).

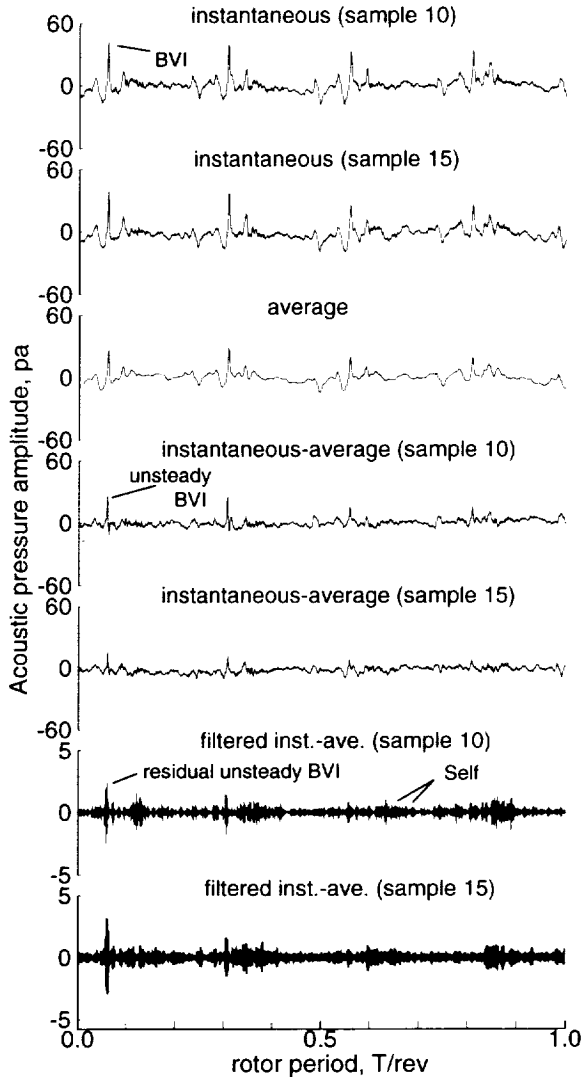

(b) Microphone location B directly under the hub (x_T=0.0m,y_T=0.0m).

Figure 6. Measured acoustic time histories for descent BVI (α=5.3°) condition. Filtered samples from 10 to 16 kHz.

noise is seen to have repetitive intensity and duration about each blade passage, although it is seen to be present throughout the rotor period. This suggests that only over limited portions of each blade's passage does Self noise contribute strongly to noise perceived by an observer at A. Figure 6(b) shows the same presentation of data for the same rotor condition, but for microphone B. Due to differing directivity effects and arrival times of noise from the various parts of the rotor, these noise signatures differ from the results of Fig. 6(a). Microphone B is directly under the rotor center and would be minimally affected by the Doppler and convective amplification effects that microphone A should observe. Figure 6(b) shows a flattening of Self noise levels and some broadening of the intense Self noise periods, compared to the microphone A.

Figure 7 shows results for a mild climb condition where broadband noise is clearly dominant over BVI noise. BVI is diminished to a non-impulsive harmonic loading noise signature. However, except for a slightly increased Self noise amplitude for mild climb, the two flight conditions show similar behavior for the same respective microphones for both BWI and Self noise. This shows that these broadband sources are somewhat less dependent on the rotor operation (angle) changes than is BVI.

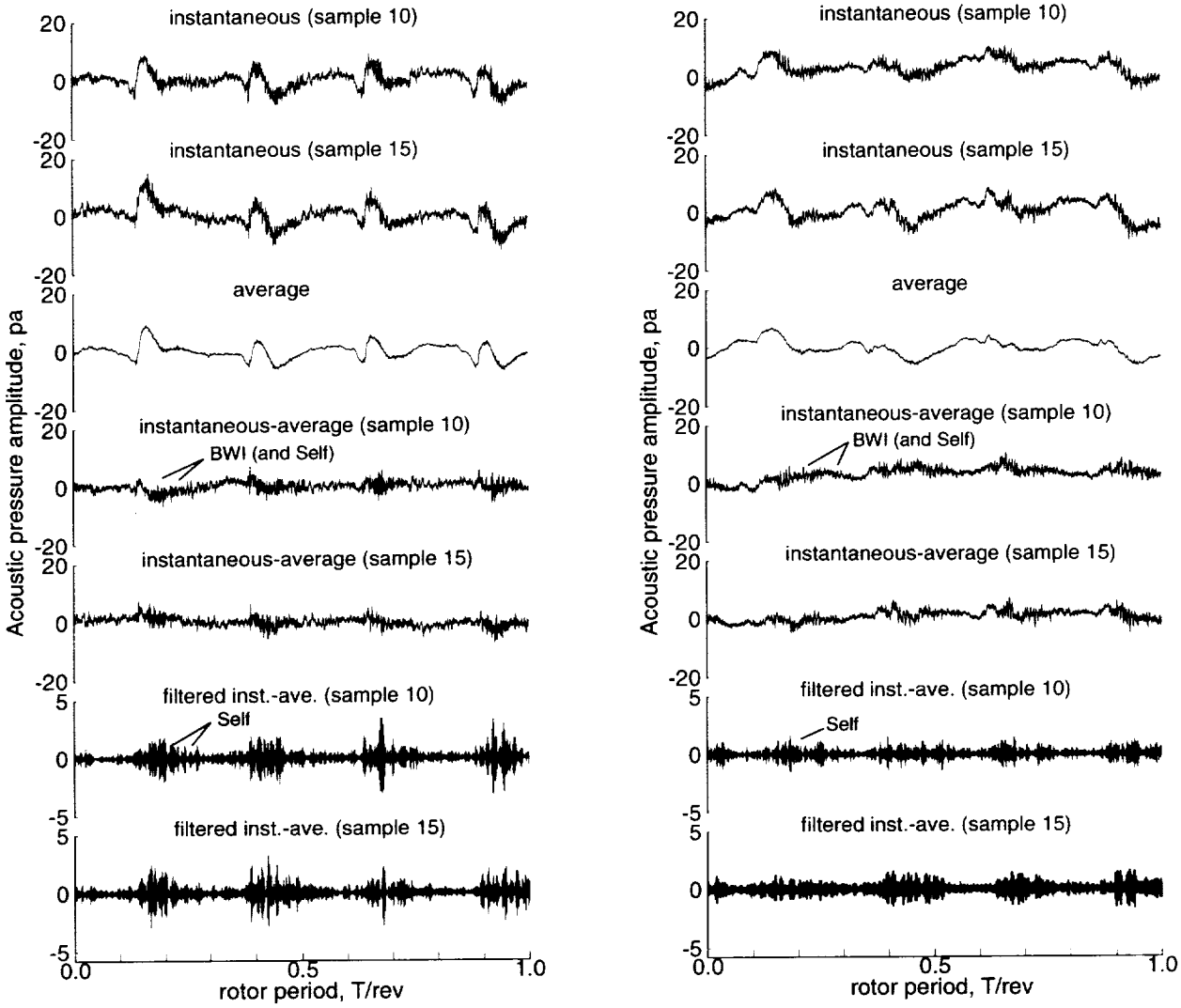

(a) Microphone location A upstream under the advancing side (x_T=2.0m,y_T=1.6m).

(b) Microphone location B directly under the hub (x_T=0.0m,y_T=0.0m).

Figure 7. Measured acoustic time histories for mild climb (α=-3.8°) condition. Filtered samples from 10 to 16 kHz.

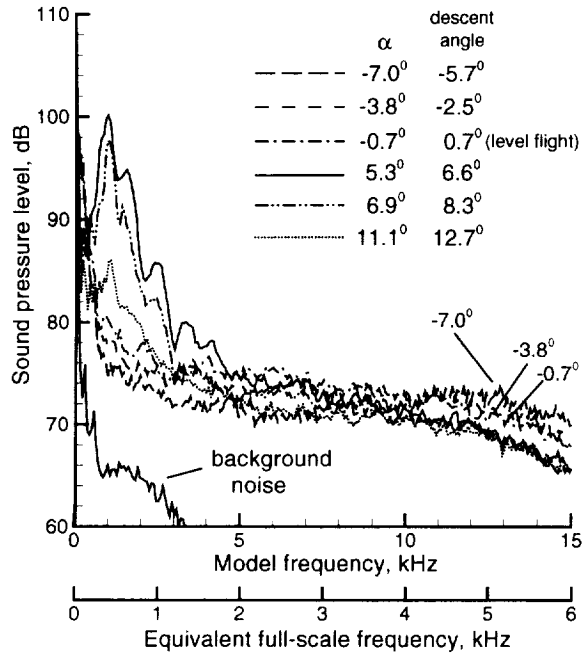

(a) Microphone location A under the advancing side (x_T=2.0m, y_T=1.6m).

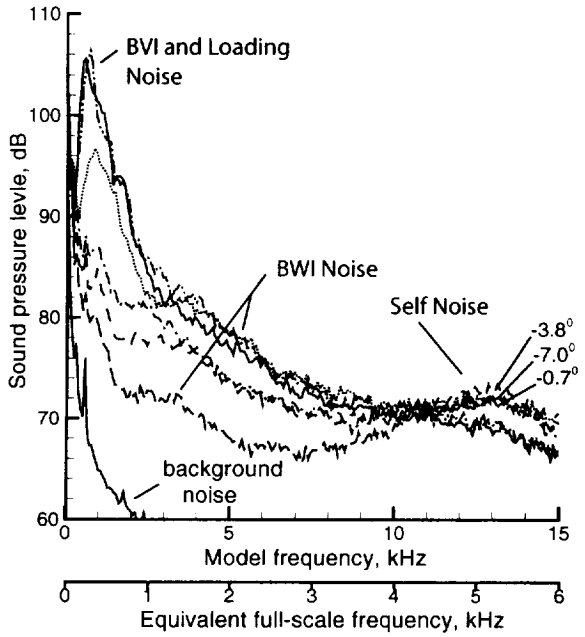

(b) Microphone location C under the advancing side (x_T=-0.5m, y_T=2.2m).

Figure 8. Measured noise spectra for a range of shaft angles (α=-7.0° to 11.1°). Resolution bandwidth is 70Hz.

Figure 8 shows spectra for a range of rotor shaft angles for forward microphone A and the side microphone C (see Fig. 5) on the rotor's advancing side. (Microphone C is chosen to demonstrate BWI noise presence in the spectra.) The spectra for $\alpha = -3.8^\circ$ and $\alpha = 5.3^\circ$ of Fig. 8(a) correspond to the forward microphone A acoustic time histories of Figs. 6(a) and 7(a). The general frequency ranges dominated by the different sources are indicated. An additional frequency scale is shown, corresponding to what an observer would hear for an equivalent full-scale rotor. The amplitude levels would be the same for an observer at the same orientation and distance compared to rotor size, r/R. A data key also shows equivalent helicopter descent angles to correspond to the shaft angle α. These serve to show the importance of broadband sources at different conditions, particularly for level and climb conditions.[8] In model scale, BWI appears prominent between about 1.5 and 6 kHz for climb conditions, whereas in descent it is prominent between about 2.5 to 7 kHz. This is more apparent for microphone C (Fig. 8(b)) than it is for microphone A. For both microphones, the Self noise spectra levels between 10 and 16 kHz appear almost invariant (constant) for climb conditions and invariant for descent conditions, all with somewhat lower levels. In Refs. 7 and 8, these lower levels were attributed to disruption of the blade boundary layers from BVI occurrences over a large portion of the rotor. But as will be shown in the next figure, directivity differences along with shaft angle changes may explain part of the level changes.

Measured Self noise directivity contours for shaft angle α variations ranging from -7.0° (climb) to +11.1° (steep descent) are shown in Fig. 9. The Self-SPL noise level metric used is the total integrated spectra between 10 and 16 kHz, and is taken to represent Self noise trends for this study. (Self noise has been shown to be significant to at least 25 kHz for this size model.[7]) As evidenced in Fig. 8, this frequency band represents a key portion of Self noise without including substantial BWI noise. The Self noise directivities show increased levels in the upstream direction on the advancing rotor side. In contrast to BVI[1] and BWI[20] noise directivity, Self noise appears somewhat invariant with rotor shaft angle. Although there is some clockwise rotation of the main directional noise lobe with increasing shaft angle, as found for BVI and BWI, the rotation is mild with slightly decreased level (less than 2 dB). It is noted that at least part of the cause of reduced levels, cited for this spectral frequency range in Fig. 8, is due to directivity changes with respect to those microphones.

NOISE PREDICTION

The prediction methodologies for BWI and Self noise sources share common implementation logic and geometric definition. Noise contributions for each source are summed from different portions (or segments) of the blade undergoing azimuthally varying flow conditions.

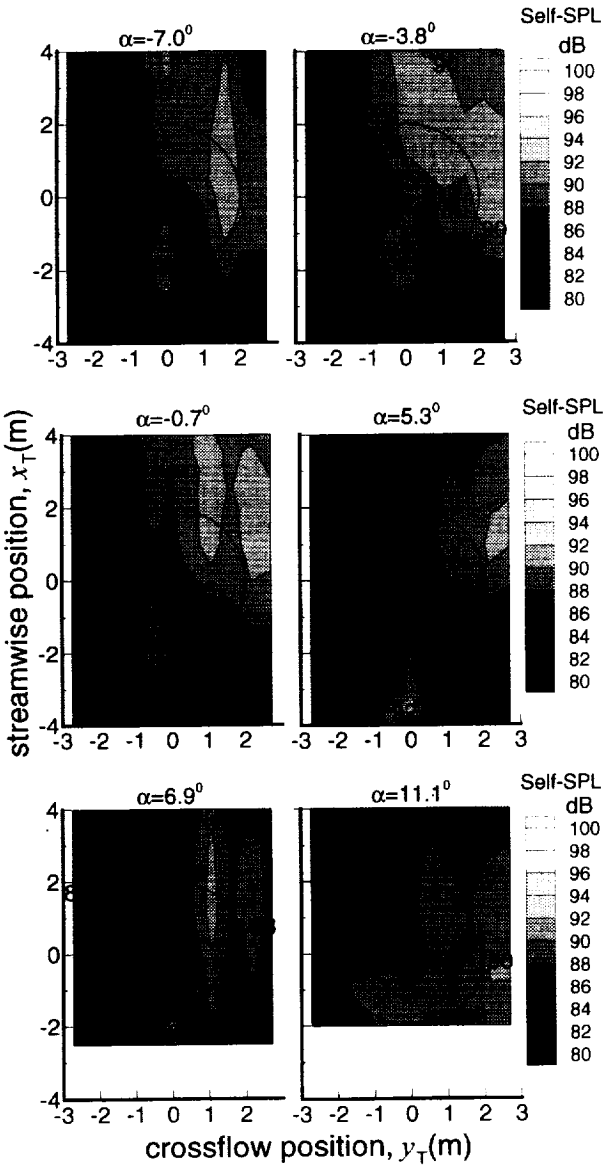

Figure 9. Measured noise contours of Self-SPL (sum of energy from 10 kHz to 16 kHz) for different rotor shaft angles over measurement plane.

Geometry

Figure 10, is a view from above the rotor, showing a blade segment positioned at radius r_m and azimuth $\Psi_n = 60^\circ$. The translational velocity at the mn^{th} segment due to rotor rotation only is designated as $\mathbf{V}_{mn}$. In this simplified picture, turbulence from the wakes of preceding blades convects at the tunnel velocity, $\mathbf{V}_{wt}$. For small rotor tip-path-plane angles α and little blade pitching or flapping, the chordwise flow speed (and convection speed of turbulent gusts in the wake) U_{mn} equals

$$U_{mn} \approx V_{mn} + V_{wt}\sin\Psi_n = \Omega r_m + V_{wt}\sin\Psi_n \qquad (12)$$

Where V_{mn} and V_{wt}, respectively, equal $|\mathbf{V}_{mn}|$ and $|\mathbf{V}_{wt}|$. In Fig. 10, the x and y axes should actually be regarded as x_{mn} and y_{mn}, but with the mn being suppressed. The x_{mn} and y_{mn} axes are of a

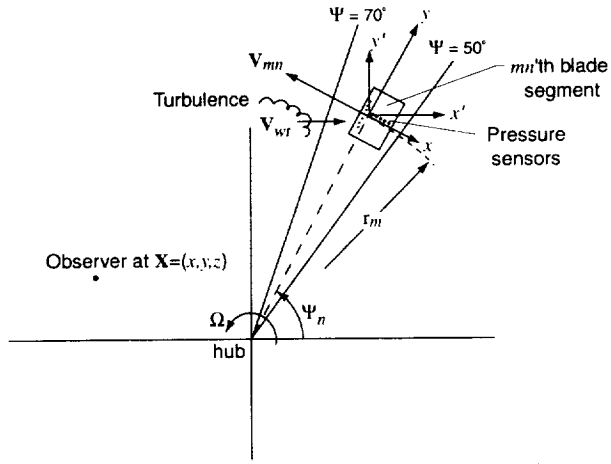

Figure 10. Blade segment at radius r_m and azimuth angle Ψ_m with translational velocity $\mathbf{V}_{mn}$ encountering turbulence that is convecting with the tunnel velocity $\mathbf{V}_{wt}$.

coordinate system $\mathbf{X}_{mn} = (x_{mn}, y_{mn}, z_{mn})$ which is positioned at the one-quarter chord and radial center of the blade segment. (Note that the $\mathbf{X}_{mn}$ coordinate origin in Ref. 20 was placed at the leading edge rather than the one-quarter chord.) A detail of the blade segment is shown in an isometric view in Fig. 11, where the mn subscript is suppressed. The x and y axes lie on the rotor disk plane with x aligned with the chordline (when the blade segment is not pitched with respect to the rotor disk). The rotor disk plane itself may or may not be tilted with respect to the tunnel. Another coordinate of interest is $\mathbf{X}'$, which has the same origin as $\mathbf{X}$, but is oriented with wind tunnel coordinates where the x' axis is aligned with the tunnel free-stream direction and z' is vertically upward. The axis z' would correspond to z if the rotor were not tilted. The coordinate $\mathbf{X}_e$ is centered at the TE with x_e and y_e in the segment's chordwise and spanwise direction, respectively. When the blade segment is pitched at angle α_p from the rotor disk plane, $\mathbf{X_e} = (x_e, y_e, z_e)$ is related to $\mathbf{X}$ by,

$$\mathbf{X_e} = (x\cos\alpha_p - z\cos\alpha_p - .75C, y, x\sin\alpha_p + z\cos\alpha_p). \qquad (13)$$

The observer (microphone) position and the velocities are defined in terms of $\mathbf{X}$, $\mathbf{X}'$, or $\mathbf{X}_e$. The components of the mean total flow velocity $\mathbf{V}_{tot}$ (*mn* subscript is suppressed) encountering the blade segment is illustrated in Fig. 11, and given by

$$\mathbf{V}_{tot} = \mathbf{V} - \mathbf{V}_{wt} - \mathbf{V}_{ind}, \tag{14}$$

where $\mathbf{V}_{ind}$ is the induced velocity due to the near and far wake of the rotor. In terms of the $\mathbf{X}_e$ coordinate, $\mathbf{V}_{tot} = (V_{tot,xe}, V_{tot,ye}, V_{tot,ze})$. The flow speed that is normal to the span is $U = (V_{tot,xe} + V_{tot,ze})$ and the aerodynamic angle of attack is $\alpha_* = \sin^{-1}(V_{tot,ze}/U)$. Note that α_* equals the pitch angle α_p if $\mathbf{V}_{wt} + \mathbf{V}_{ind} = 0$. Normally, a rotor trim code such as CAMRAD.Mod1 would determine U and α_p as part of its iterative trim calculations.

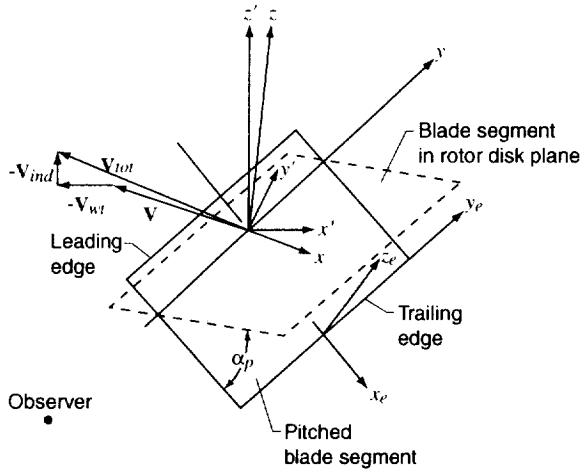

Figure 11. The blade segment of Fig. 10 detailing coordinate systems with respect to blade pitch and orientation to components of the incoming flow field. The subscript *mn* is suppressed for clarity.

As shown in Figs. 10 and 11, each mn^{th} blade segment is skewed and pitched with respect to the windtunnel flow in which it is submersed. In Fig. 12, the blade segment is on the tilted rotor disk referenced to the $\mathbf{X}'$ coordinate system. As in shown in Fig. 11, x' is aligned with $\mathbf{V}_{wt}$. (In the present modeling for broadband noise radiation, the disk is not considered to have coning or higher-order flapping.) The effect of the tunnel flow on noise radiation can be important. As illustrated in Fig. 12, any noise emitted from the blade segment location would appear to the observer to be emitted from a more downstream location due to the convection of

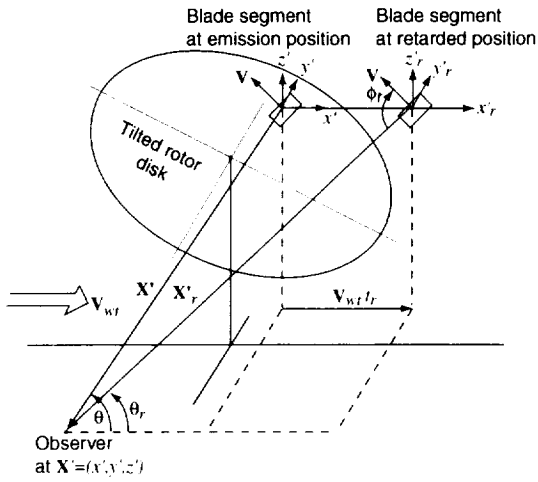

Figure 12. Blade segment on rotor disk in tunnel showing emission and retarded coordinates.

the sound field within the tunnel flow at velocity $\mathbf{V}_{wt}$. Specifically, the blade segment is at an emission distance $|\mathbf{X}'|$ from the observer at $\mathbf{X}'$, but appears to be at a "retarded" position at a distance $|\mathbf{X}'_r|$. The propagation time is $t_r = |X'_r|/c_0$. The TE coordinates $\mathbf{X}_e$ can also be referenced to a "retarded" position at a distance $r_{er} = |\mathbf{X}_{er}|$, by noting that the relationship previously given between $\mathbf{X}_e$ and $\mathbf{X}$ also holds between $\mathbf{X}_{er}$ and $\mathbf{X}_r$. These convective effects must be included in order to properly determine noise directivity, Doppler frequency shifting, and convective acoustic pressure amplification.

BWI noise source strength calculations

In Burley, et al.[20] for BWI noise prediction, the turbulence itself was not modeled, but was accounted for in a surface dipole acoustic modeling approach through measured blade pressures. Figure 10 illustrates the rotor blade segment, instrumented with unsteady pressure sensors, encountering turbulence. The measured surface pressure differences Δp between the lower and upper surfaces of the blade permit the cross-spectra to be determined and modeled. This is used with acoustic theory to predict the noise spectrum at observer positions. The BWI noise spectral contribution from the mn^{th} blade segment was found to be, in present terminology,

$$G_{BWI}(f) = \left(\frac{\omega z_r}{4\pi c_0 \sigma^2}\right)^2 G_{LE\Delta p}(f) \cdot [bC]^2 \left(\frac{2L(\varsigma\omega/U)}{(\varsigma\omega/U)^2 + (\omega y_r/c_0\sigma)^2}\right). \tag{15}$$

Equation (15) is in a more explicit form than that given in Ref. 20. The frequency is $\omega = 2\pi f$ and c_0 is the speed of sound in the medium. The subscripts on y_r and z_r indicate components of the retarded coordinates $\mathbf{X}_r$. The term

$$\sigma^2 = |\mathbf{X}_r|^2 (1 - M_{tot} \cos\xi_r)^2 \tag{16}$$

where

$$M_{tot} = V_{tot}/c_0 = |\mathbf{V}_{tot}|/c_0, \tag{17}$$

($\mathbf{V}_{ind}$ is assumed small compared to $\mathbf{V}_{tot}$) and

$$\cos\xi_r = \mathbf{X}'_r \cdot \mathbf{V}_{tot} / (|\mathbf{X}'_r| V_{tot}). \tag{18}$$

$G_{LE\Delta p}(f)$ is the auto-spectrum of the unsteady pressure differential near the leading edge (taken as 3 percent chord from the LE in Ref. 20). The segment chordlength is C and the span is L. The factors b and ζ are constants related to the chordwise and spanwise length scales of the blade response to turbulence, based on cross-spectral measurements. A small value of b would indicate that the blade-loading response to inflow turbulence is concentrated only near the leading edge. A large value of ζ would indicate small spanwise correlation length scales for blade loading. The term containing y_r accounts for acoustic non-compactness, with respect to the observer, which is associated with the spanwise loading distribution. For this paper, the BWI noise predictions are performed in the same manner as that in Ref. 20.

Self noise source strength calculations

For Self noise prediction, Eqs. (1)-(11) define the basic contributions from each mn^{th} blade segment. The velocity, boundary layer, and scale input parameters used in the previous main rotor model application[7] are described in Appendix C of Ref. 27. For that study, the same model BO-105 blade section design is also that of the present HART test. In the present paper, however, there are several major prediction application differences. One is that the rotor performance / trim code CAMRAD.Mod1 /HIRES is used to better define the blade segment velocities and angles. Another is that the more general geometric and convective field definitions (given above) and the expanded database of HART permit for the first time an evaluation of predicted Self noise directivity. (The previous study used only a single on-axis microphone position.) This permits an examination of source amplitude, directivity, and frequency dependence on blade segment and tunnel Mach numbers, as well as some evaluation of the possible role of local incidence flow unsteadiness on the validity of the quasi-steady assumptions of the Self noise prediction modeling.

The directivity functions $\bar{D}_l$ (for low frequency sources) and $\bar{D}_h$ (for high frequency sources) are, for the present study

$$\bar{D}_l = \frac{\sin^2\Theta_{er} \sin^2\Phi_{er}}{(1 - M_{tot}\cos\xi_r)^4} \tag{19}$$

and

$$\bar{D}_h = \frac{2\sin^2(\Theta_{er}/2)\sin^2\Phi_{er}}{(1 - M_{tot}\cos\xi_r)^4} \tag{20}$$

where the flyover and sideline angles (with respect to the tilted segment TE of Fig. 11) are, respectively,

$$\Theta_{er} = \cos^{-1}(x_{er}/r_{er}),$$
$$\Phi_{er} = \cos^{-1}(y_{er}/(y_{er}^2 + z_{er}^2)^{1/2}) \tag{21}$$

with

$$r_{er} = |X_{er}| = (x_{er}^2 + y_{er}^2 + z_{er}^2)^{1/2}. \tag{22}$$

Equation (19) for $\bar{D}_l$ is the same as recommended in Ref. 27, but is now defined based on conditions of Fig. 12. This assumes that the offset in distance of the trailing edge compared to one-quarter chord is inconsequential to the observer angle definition, which is true in the far-field of the blade segment. Note that the directivity represented in Eq. (15) for BWI noise approaches that of Eq. (19) when ζ is large (implying compact loading for BWI). For $\bar{D}_h$, the numerator in Eq. (20) has the expected cardioid pattern for trailing edge noise. The denominator in Eq. (20) is the same as that in Eq. (19), however, it represents a somewhat stronger Doppler/convective amplification factor than that suggested (but not validated) in Ref. 27. Amplification factors have been a concern of different theoretical approaches[47,48,49] for the TBL-TE problem for low to moderate Mach numbers. Different "effective" exponent power laws between 1.5 and 4.5 have been found. There have not been validations for any meaningful higher Mach number or angle ranges[28,23]. The 4th power of Eq. (20) is commonly accepted for compact dipole sources[50] and is applied here for all high-frequency Self noise sources, not just the TBL-TE noise source.

Boundary-layer definition. With the local blade segment velocity U and angle α_* determined by CAMRAD.Mod1, the BL equations from Ref. 27

are applied using the untripped BL case. The α_* used is the aerodynamic angle of attack. This is referenced to the zero lift angle, which is -1.4° from the chordline (or geometric) angle of attack for the NACA 23012 airfoil.

TBL-TE noise prediction. With the definition of the segment geometry, boundary layer displacement thicknesses, U, and α_*, the basic G_{TBL-TE} noise calculation is accomplished using Eq. (2). However, although not done in Ref. 7, a Glauert-Prandtl type correction for compressibility effects is applied. This type of correction is proven to give good first order approximation to account for the effect of Mach number on pressures over airfoil surfaces[51]. The value of mean pressures P over airfoil surfaces, referenced to the mean stream pressure P_∞, is related to that found for incompressible low-speed flow by $P-P_\infty=(P-P_\infty)_{lowspeed}/\beta$, where $\beta=(1-M^2)^{1/2}$. Assuming mean and turbulent flow similarity at higher speeds, one obtains for unsteady surface pressure

$$p'=p'_{lowspeed}/\beta, \tag{23}$$

therefore, the predicted noise spectrum is corrected to be

$$G_{TBL-TE,cor}=G_{TBL-TE}/\beta^2. \tag{24}$$

While the above analysis is not rigorous, as issues of scale and local compressibility effects with regard to noise production need to be addressed, such increases of levels suggested by Eq. (24) should be anticipated. For the present study, rotor blade segments on the advancing side approach a Mach number of $M=.75$. The scaling leading to G_{TBL-TE} is based on isolated airfoil data limited to a Mach number of $M=.21$. From $M=.21$ to approximately $M=.6$, flow similarity should hold and Glauert-Prandtl relations should apply. Between approximately $M=.6$ and .75, supercritical flow occurs over the surface and shocks develop, which lead to disrupted (non-similar) boundary layer flow. Although from a mean loading standpoint, the Glauert-Prandtl relations should still generally hold[51], it is uncertain to what extent Eq. (24) applies because of the breakdown in similarity. From a surface pressure standpoint, Eq. (23) defines the assumed unsteady loading near the trailing edges. Unfortunately in the present study, pertinent high-frequency unsteady surface pressure data are not available for confirmation.

LBL-VS noise prediction. Given the segment geometry, BL thicknesses, U, and α_*(geometric angle referenced to the chordline), the basic G_{LBL-VS} noise calculation is accomplished using Eq. (9). As previously stated, the boundary layer calculations employ the aerodynamic angle. As recommended in Ref. 27, the LBL-VS noise production is limited to rotor regions where the blade segments are determined to encounter smooth and un-skewed inflow. These criteria require contributions from other region to be zeroed (or nulled). The controlling mechanism of LBL-VS noise is the presence of aeroacoustic feedback loops created between the trailing edge and an upstream location on the airfoil surface where laminar instabilities occur. Criteria are based on the premise that the presence of sufficiently unsteady flow conditions over portions of the rotor would prevent the establishment of the mechanism and related noise. The "unsteadiness" criterion presently employed depends on an examination of the high-resolution deterministic far-wake (without near-wake) inflow to each blade segment over each 20° azimuth range that it represents. The actual spanwise width of the arch area examined equals one chordlength. This employs an intermediate output of the HIRES code, represented in Fig. 2. LBL-VS noise is taken to contribute only when the root-mean-square values of flow upwash non-uniformity are below 1% of U (this is analogous to turbulent intensity). The "skew" criterion allows LBL-VS noise contributes when the flow-skew-angle over each segment is less than 15°. This serves to null regions immediately upstream and downstream of the hub. The choices of these criteria are examined subsequently.

BTE noise prediction. Following Ref. 27 in evaluating Eq. (10), the trailing edge thickness h is given as .9mm, the solid trailing edge angle ψ is 14°, and .5mm is added to the calculated value of δ^*_{avg} to account for a .5mm step that is 5mm upstream of the TE. Also, as recommendated in Ref. 27 (based on the rotor RPM study of Ref. 7) the BTE noise contribution is limited to Mach numbers below .5 at each blade segment.

Tip noise prediction. Equation (11) is evaluated for the flat edge tip condition in the manner of Appendix C of Ref. 27, with the exception that α_{Tip} is defined as the local flow angle-of-attack, but without the near-wake contribution, in order to more accurately represent the test conditions on which Ref. 27 is based. The local flow angles were found through the HIRES code of Fig. 2.

Total noise calculations

The calculation and summation of BWI and Self noise from the methods above, accounting for Doppler frequency shifts, produces an "instantaneous" spectrum for the noise radiated to the observer from the blade segment located at the mn^{th} position. The next step of summing the noise from all

blade segments at the observer involves frequency bandwidth adjustments and spectral weighting.

The knowledge of $\mathbf{X}'_r$ and $\mathbf{V}$ allows for the determination of the Doppler shift in frequency due to the relative motion of the mn^{th} blade segment with respect to the observer in the presence of the tunnel mean flow. This factor simply stretches or contracts the noise spectra frequency-wise by the ratio of the Doppler-shifted frequencies, f_0, compared to the un-shifted frequencies, f. Note that before accounting for Doppler shifts, the frequency resolution of the $G_{BWI}(f)$ noise spectrum of Eq. (15) is the same as that of the $G_{LE\Delta p}(f)$ spectrum at each mn^{th} position. Also, since Self noise is calculated in one-third Octave bands, it is converted to the bandwidth resolution of the BWI data, assuming a linear level distribution of noise between one-third Octave center-frequencies. With Doppler shifting, this frequency resolution bandwidth is

$$(\Delta f)_{T_0} = (360^\circ/\Delta\Psi)(f_0/f)(\Delta f)_T, \qquad (25)$$

where $(\Delta f)_T$ is the bandwidth of spectra based on a data azimuth range (360°) of one rotor period T, and $\Delta\Psi$ is the azimuth range (20°) over which the data was processed for the mn^{th} segment.

The final summation for the total broadband noise at each observer is done with the common bandwidth $(\Delta f)_T$ based on the rotor period T. An energy-preserving algorithm was developed to put the individual spectrum on this common spectral basis. The resulting spectra for each mn^{th} segment are designated as $\left[G_{BWI}(\mathrm{f})\right]_{mn}$ and $\left[G_{Self}(\mathrm{f})\right]_{mn}$, where f is used to signify that the spectra are the result of this frequency processing. The total broadband noise at the observer is

$$G_{BB}(\mathrm{f}) = \sum_{m=1}^{m_0} \sum_{n=1}^{360^\circ/\Delta\Psi} 4\left(\frac{\Delta\Psi}{360^\circ}\right)\left(\frac{f}{f_0}\right)_{mn} \cdot \left\{\left[G_{BWI}(\mathrm{f})\right]_{mn} + \left[G_{Self}(\mathrm{f})\right]_{mn}\right\}. \qquad (26)$$

Here, the effects of 14 radial stations (BWI calculations include only the outer 9 stations where pressure measurements were made) and all $(360^\circ/\Delta\Psi) = 18$ azimuthal ranges, for $\Delta\Psi = 20^\circ$, are summed. The weighting factors include 4 for the number of blades. The terms $(\Delta\Psi/360^\circ)(f/f_0)_{mn}$ account for the portion of time spent in each mn range, compared to one rotor revolution, as seen acoustically by the observer at $\mathbf{X}$. The actual proportional time spent is $(\Delta\Psi/360^\circ)$, whereas $(f/f_0)_{mn}$ is a correction factor to account for time compression/expansion effects due to blade motion and tunnel flow speed. This $(f/f_0)_{mn}$ equals the inverse of the Doppler factor (f_0/f) determined for the mn^{th} segment.

Source distributions. Contributions to the total predicted broadband noise $G_{BB}(\mathrm{f})$, Eq. (26), from the Self noise sources, $G_{LBL-VS}(\mathrm{f})$, Eq. (9), and $G_{TBL-TE,cor}(\mathrm{f})$, Eq. (24), are presented by Self-SPL level contours over the rotor disk in Fig. 13 for two rotor operating conditions. The grid-line intersections correspond to the mean segment mn locations. The calculations are made for an observer at forward microphone A. (Because of directivity effects, calculations made for other observer locations would render different distributions.) Only two source distributions are presented because, as will be seen, they dominate the predicted Self noise. The TBL-TE noise contributions are seen to be concentrated on the outer portion of the rotor disk, where blade segment velocities are highest relative to both the local flow and relative to the microphone. The TBL-TE contributions appear almost invariant between the

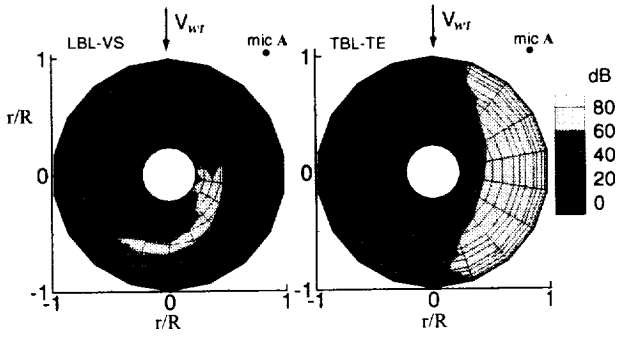

(a) Mild climb (α=-3.8°) condition.

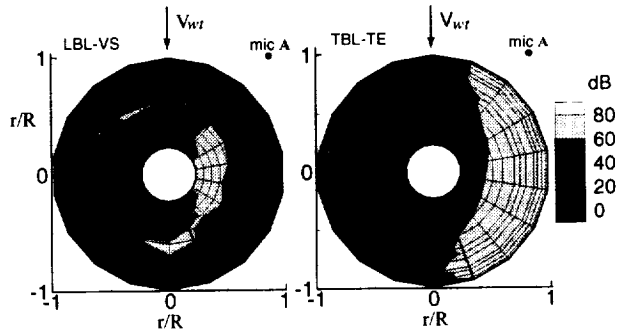

(b) BVI descent condition (α=-5.3°).

Figure 13. Distribution of different Self noise (sum of energy from 10 to 16 kHz) contributions to Self-SPL over the rotor disk for forward microphone location A (x_T=2.0m, y_T=1.6m).

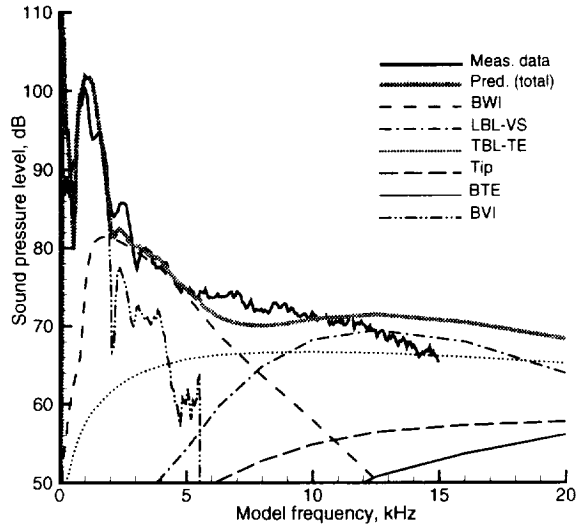

(a) Microphone location A (x_T=2.0m, y_T=1.6m).

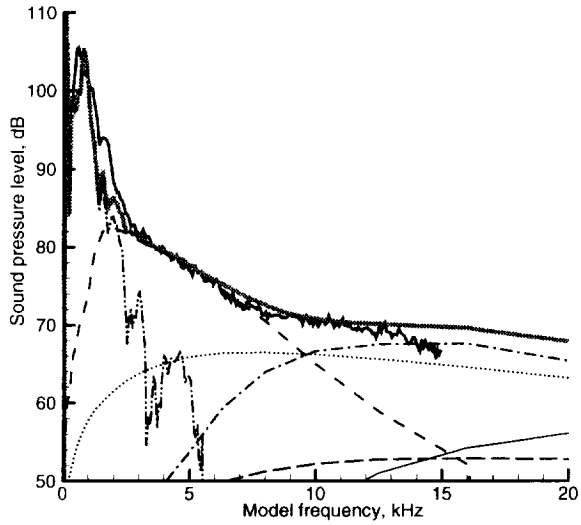

(b) Microphone location C (x_T=-0.5m,y_T=2.2m).

Figure 14. Measured and predicted noise spectra for descent condition (α=-5.3°). The bandwidth is 70Hz.

mild-climb and descent conditions shown. The LBL-VS noise contributions are seen to be stronger more inboard, where LBL's would tend to exist over extended portions of the blade segments. Substantial parts of the rotor disk are seen to be nulled per the unsteadiness criteria defined in the last section. The criterion that the cyclic flow-skew-angle is less than 15° nulls the regions immediately upstream and downstream of the hub. The flow unsteadiness criterion of 1% is seen to eliminate regions where wake vortices are present. This nulling leaves strong LBL-VS contributions from inboard regions on the advancing side, along with aft rotor disk regions for the mild-climb condition and forward rotor disk regions for the descent condition.

Comparison with Measurements

Predicted and measured spectra for the forward microphone A and side microphone C are shown in Fig. 14 for a high BVI descent condition.

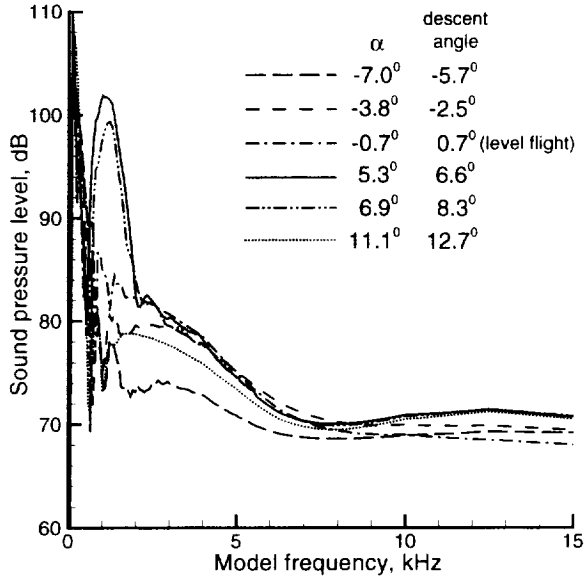

(a) Microphone location A (x_T=2.0m, y_T=1.6m).

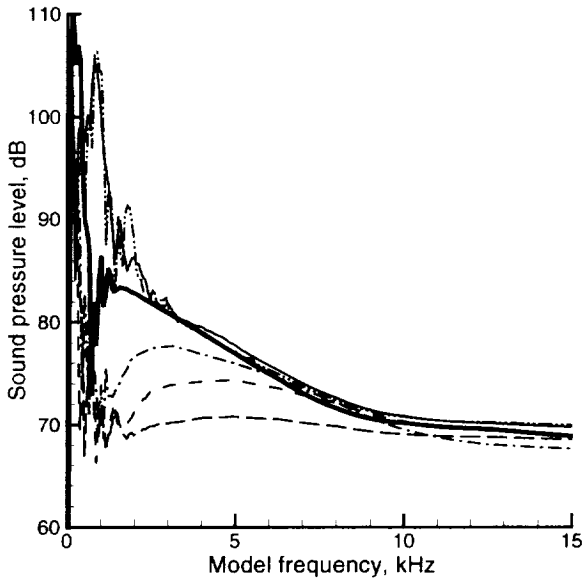

(b) Microphone location C (x_T=-0.5m,y_T=2.2m).

Figure 15. Predicted noise spectra for shaft angles (α=-7.0° to 11.1°). The bandwidth is 70Hz. (Corresponds to data of Fig. 8)

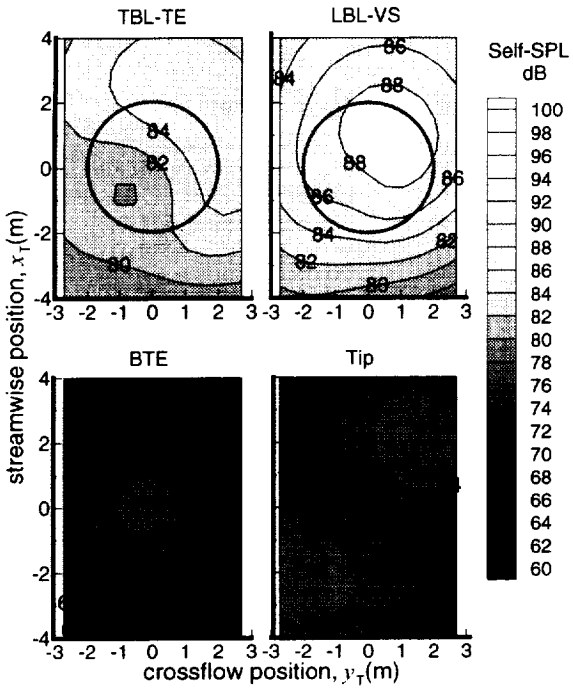

Figure 16. Predicted contribution contours of Self-SPL (sum of energy from 10kHz to 16kHz) for four different Self noise mechanisms for a BVI descent condition, α=-5.3°.

The total prediction is the sum of harmonic and BVI noise[1] and broadband noise, with BWI and individual Self noise contributions. Overall, the agreement between measurement and prediction is quite good. The BWI prediction appears to properly explain the mid-frequency range when the BVI levels diminish at about 2.5 kHz. Self noise begins to dominate the spectra beyond about 8 kHz. The TBL-TE noise has broad spectral content over the frequency range, while LBL-VS noise is more peaked in the higher frequencies. Tip and BTE noise predictions are seen not to contribute significantly to the total spectra. The total predicted noise spectra for the range of rotor shaft angles are given in Fig. 15 for the same two microphones of Fig. 14. When compared to the measured spectra of Fig. 8, one can see substantial agreement in spectral shape as well as level. This represents the first "complete" spectral prediction-measurement comparison for main rotor noise, to the knowledge of the authors. It is noted that the method does not appear to capture all the trend details of the high-frequency Self noise levels with shaft angle change. But as noted earlier, with regard to Fig. 8 for the two microphones, much of the difference can be attributed to directivity changes not properly captured.

Figure 16 shows predicted Self-SPL directivity contours of the four individual sources for the descent condition of Fig. 14. It is seen, as with the spectral presentations, that TBL-TE and LBL-VS noise dominate that of BTE and Tip noise. The most intense levels appear on the forward advancing side. The total predicted Self-SPL contours for rotor shaft angle variations are shown in Fig. 17. The contour shapes and levels do not vary drastically with angle. In comparing this with measured contours of Fig. 9, one sees good agreement in level and nominal directivity, but only fair agreement in directivity trends.

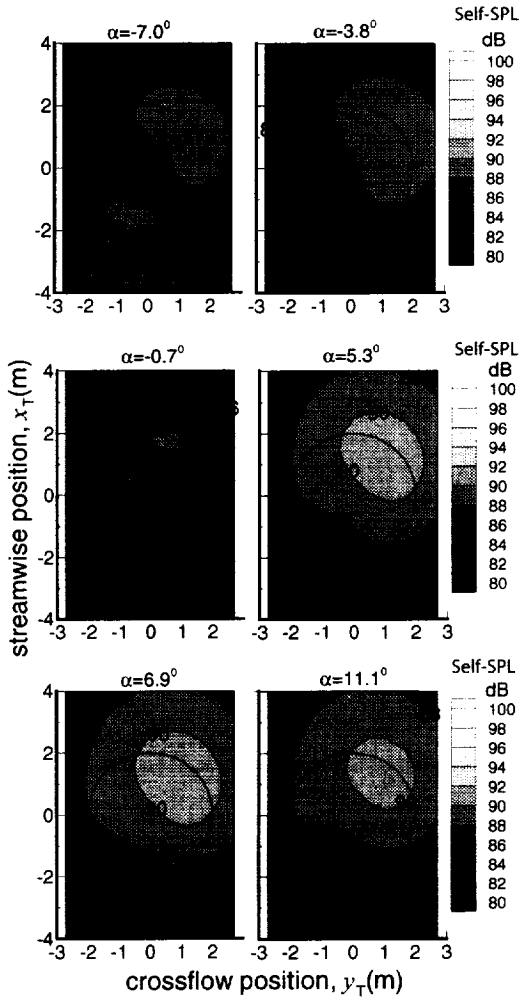

Figure 17. Predicted contours of total Self-SPL (sum of energy from 10kHz to 16kHz) for different rotor shaft angles. (Corresponds to the data of Fig. 11)

COMMENTS

The above prediction success follows from (1) the application of scaling and input recommendations of Ref. 27 (based on the study of Ref. 7), (2) the accounting for acoustic effects - including local blade source directivity, convective and Doppler amplification, Doppler frequency shifts and spectral summing, and (3) the accounting for anticipated

source strength dependence on compressibility and flow unsteadiness. To further improve the predictions, a number of key issues or questions should be addressed. One is the evaluation of directivity modeling for the sources associated with the different flow states. Another important evaluation is that of TBL flow similarity and pressure loading for flow approaching transonic speeds. For example, as mentioned in the text, the presence and cyclic movement of shocks over the blade surface could alter the flow and appropriate noise modeling substantially. Specific surface pressure measurements and flow field data are needed to validate the presently assumed flow field over the blade surface. An equally important issue is that of proper criteria to determine the presence of the LBL-VS noise mechanism. This mechanism can produce intense levels but has been found to depend on ideal flow conditions where LBL flow can persist in a quasi-steady manner and establish Tollmien-Schlichting instability waves[52], which have been postulated to be essential for the creation of the acoustically excited aerodynamic feedback loops[27,30]. Inflow turbulence, boundary layer tripping, or high Re_c conditions null this mechanism[24,27]. The present criteria assume that cyclic skew flow and flow-unsteadiness (due the presence of a vortex) near the blade segment would interrupt the mechanism. However, the criteria evaluation depends only on the deterministic output from CAMRAD.Mod1/HIRES, and does not include a turbulence inflow model. It is likely that improved criteria would include a connection to some future BWI modeling that establishes turbulence definition over the wake.

CONCLUSIONS

The present study shows the development and validation of broadband Self noise prediction methodology for rotors. Combined with predictions of harmonic and BVI noise and broadband BWI noise, the first predictions of complete noise spectra are compared to that measured for a main rotor. The Self noise prediction method employs scaled results from isolated non-rotating airfoil segments, advanced rotor performance codes to determine local blade segment flow conditions, as well as acoustic and aerodynamic modeling to account for source strength and noise radiation dependence on flow and blade definition. The present prediction coding is robust. Good agreement with data is found in noise level (within several dB) and nominal directivity for rotor conditions ranging from descent to climb. Areas of further study for prediction model refinement are identified.

ACKNOWLEDGEMENTS

The authors would like to thank all other members of the HART team from AFDD, DLR, ONERA, and DNW for their continuous efforts before, during, and after the HART test program.

REFERENCES

1. Brooks, T.F., Boyd, D.D. Jr., Burley, C.L., and Jolly, J.R.Jr., "Aeroacoustic Codes for rotor Harmonic and BVI Noise – CAMRAD.Mod1/HIRES", *Journal of American Helicopter Society*, April 2000, pp. 63-79.

2. Burley, C.L., Brooks, T.F., Marcolini, M.A., Brand, A.G., and Conner, D.A., "Tiltrotor Aeroacoustic Code (TRAC) Predictions and Comparisons with Measurement," *Journal of American Helicopter Society*, April 2000, pp. 80-89.

3. JanakiRam, R.D. and Khan, H., "Prediction and Validation of Helicopter Descent Flyover Noise," 56th AHS Annual Forum, Virginia Beach, VA, May 2-4, 2000.

4. Burley, C.L., Brooks, T.F., Charles, B.D., and McCluer, M., "Tiltrotor Aeroacoustic Aeroacoustic Code (TRAC) Prediction Assessment and Initial Comparisons with TRAM Test Data," 25th European Rotorcraft Forum, Paper B3, Rome, Italy, Sep. 14-16, 1999.

5. Boyd, D.D. Jr. and Burley, C.L., "Analysis of Measured and Predicted Acoustics from an XV-15 Flight Test," 57th AHS Annual Forum, Washington, D.C., May 9-11, 2001.

6. Prichard, D.S., "Initial Tiltrotor Aeroacoustic Code (TRAC) Predictions for the XV-15 Flight Vehicle and Comparison with Flight Measurement," 56th AHS Annual Forum, Virginia Beach, VA, May 2-4, 2000.

7. Brooks, T. F., Marcolini, M. A., and Pope, D. S., "Main Rotor Broadband Noise Study in the DNW," *Journal of American Helicopter Society*, vol 34, no. 2, April 1989, pp. 3-12.

8. Brooks, T. F., Jolly, J. R. Jr., and Marcolini, M. A., "Helicopter Main Rotor Noise: Determination of Source Contribution using Scaled Model Data," *NASA TP* 2825, Aug. 1988.

9. Johnson, W., "A Comprehensive Analytical Model of Rotorcraft Aerodynamics and Dynamics, Part 1- Analysis and Development," *NASA TM*-81182, June 1980.

10. Brentner, K.S., "Prediction of Helicopter Rotor Discrete Frequency Noise," *NASA TM* 87721, Oct. 1986.

11. Beddoes, T.S., "Two and Three Dimensional Indicial Methods for Rotor Dynamic Airloads," AHS National Specialists Meeting on Rotorcraft Dynamics, Arlington, TX, Nov. 1989.

12. Beddoes, T.S., "A Near Wake Dynamic Model," AHS Specialists Meeting on Aerodynamics and Aeroacoustics, Arlington, TX, Feb. 1987.

13. Farassat, F., and Myers, M.K., "Extension of Kirchhoff's Formula To Radiation from Moving Surfaces," *Journal of Sound And Vibration*, vol. 123, no. 3, 1988, pp. 451–461.

14. Glegg, S. A. L., "Prediction of Blade Wake Interaction Noise Based on a Turbulent Vortex Model," *AIAA Journal*, vol. 29, no. 10, 1991, pp. 1545-1551.

15. Amiet, R.K., "Acoustic Radiation From an Airfoil in a Turbulent Stream," *Journal of Sound and Vibration*, 41(4), pp. 407-420, 1975.

16. Glegg, S. A. L., Devenport, W.J., Wittmer, K.S., and Pope, D.S., "Broadband Helicopter Noise Generated by Blade Wake Interactions," AHS Technical Specialists' Meeting For Rotorcraft Acoustics and Aerodynamics, Williamsburg, Virginia, October 28-30, 1997.

17. Wittmer, K.S. Devenport, W.J., Rife, M.C., and Glegg, S.A.L., "Perpendicular Blade-vortex Interaction," *AIAA Journal*, vol 33, no. 9, September 1995, pp. 1667-1674.

18. Wittmer, K.S. and Devenport, W.J., "The Effects of Perpendicular Blade Vortex Interaction, Part 1: Turbulence Structure and Development," *AIAA Journal*, vol. 37, no. 7, July 1999, pp. 805-812.

19. Wittmer, K.S., Devenport, W.J., and Glegg, S.A.L., "The Effects of Perpendicular Blade Vortex Interaction , Part 2: Parameter Study," *AIAA Journal*, vol. 37, no. 7, July 1999, pp. 813-817.

20. Burley, C. L., Brooks, T. F., Splettstoesser, Schultz, K.-J., W. R., Kube, R., Bucholtz, H., Wagner, W., and Weitemeyer, W., "Blade Wake Interaction Noise For A BO-105 Model Main Rotor," AHS Technical Specialists' Meeting For Rotorcraft Acoustics and Aerodynamics, Williamsburg, VA, October 28-30, 1997

21. Brezillon, J., Prieur, J., and Rahier, G., "Investigation on Broadband Helicopter Rotor Noise," AHS Technical Specialists' Meeting For Rotorcraft Acoustics and Aerodynamics, Williamsburg, VA, October 28-30, 1997.

22. Brooks, T. F. and Schlinker, R.H., "Progress in Rotor Broadband Noise Research," *Vertica*, vol. 7, no. 4, 1983, pp. 287-307.

23. Brooks, T. F. and Hodgson, T.H., "Trailing Edge Noise Predictions Using Measured Surface Pressures," *Journal of Sound and Vibration*, vol 78, 1981.

24. Brooks, T. F. and Marcolini, M. A., "Scaling of Airfoil Self Noise Using Measured Flow Parameters," *AIAA Journal*, vol. 23, Feb 1985.

25. Brooks, T. F. and Marcolini, M. A., "Airfoil Tip Vortex Formation Noise," *AIAA Journal*, vol. 24, Feb 1986.

26. Brooks, T. F., Marcolini, M. A., and Pope, D. S., "Airfoil Trailing Edge Flow Measurements," *AIAA Journal*, vol. 24, Aug. 1986.

27. Brooks, T. F., Pope, D. S., and Marcolini, M. A., "Airfoil Self-Noise and Prediction," *NASA RP* 1218, July 1989.

28. Schlinker, R.H. and Amiet, R.K., "Helicopter Rotor Trailing Edge Noise," *NASA CR*-3470, 1981, (See also AIAA Paper 81-2001.)

29. Schlinker, R.H., "Airfoil Trailing Edge Noise Measurements with a Directional Microphone," AIAA Paper 77-1269, Oct. 1977.

30. Fink, M.R., Schlinker, R.H., and Amiet, R.K., "Prediction of Rotating-Blade Vortex Noise from Noise of Non-Rotating Blades," *NASA CR*-2611, 1976.

31. Ffowcs Williams, J.E. and Hall, L.H., "Aerodynamic Sound Generation by Turbulent Flow in the Vicinity of a Scattering Half Plane," *Journal of Fluid Mechanics*., vol. 40, no. 4, Mar. 1970, pp. 657-670.

32. Golub, R.A., Weir, D.S., and Tracy, M.B., "Application of the Baseline Rotonet System to the Prediction of Helicopter Tone Noise," AIAA Paper No. 86-1904, Jul. 1986.

33. Wagner, S., Bareiss, R., and Guidati, G., *Wind Turbine Noise*, Springer-Verlag, Berlin Heidelberg, 1996.

34. Lowson, M.V., "Applications of Aero-Acoustic Analysis to Wind Turbine Noise Control," *Wind Engineering*, vol. 16, no. 3, pp. 126-140, 1992.

35. Lowson, M.V., Fiddes, S.P., Kloppel, V., et al., "Theoretical Studies Undertaken During the Helinoise Programme," 19th European Rotorcraft Forum, pp. (B4) 1-8, Sep. 1993.

36. Lowson, M.V. and Lowson, J.V., "Systematic Comparison of Predictions and Experiment for Wind Turbine Aerodynamic Noise," Flow Solutions Report 93/03, ETSU W/13/00363/REP, pp. 1-18, Apr. 1993.

37. Lowson, M.V., "Theory and Experiment for Wind Turbine Noise," AIAA Paper 94-0119, 32nd Aerospace Sciences Meeting and Exhibit, pp. 1-9, Jan. 1994.

38. Pettersson, F., "Prediction of Broadband Noise from Wind Turbines with Sawtooth Trailing Edges," FFA TN 1993-49, pp. 1-62, Nov. 1993.

39. Bareiss, R., Guidati, G., and Wagner, S., "An Approach Towards Refined Noise Prediction of Wind Turbines," *Proc. of the European Wind Energy Association Conf. & Exhibition*, Dr. J.L. Tsipouridis (ed), Thessaloniki, vol. 1, pp. 785-790, Oct. 1994.

40. Glegg, S.A.L. and Jochault, C., "Broadband Self Noise from a Ducted Fan," AIAA Paper 97-1612, 3rd AIAA/CEAS Aeroacoustics Conference, Atlanta, GA, May 12-14, 1997.

41. Glegg, S.A.L., "Broadband Fan Noise Generated by Small Scale Turbulence," Final Report on NASA Grant NAG 1-1202, C.A.V., Florida Atlantic University, Apr. 1998.

42. Amiet, R.K., "Noise Due to Turbulent Flow Past a Trailing Edge," *Journal of Sound and Vibration*, vol. 47, pp. 387-393, 1976.

43. Yu, Y. H., Gmelin, B., Heller, H., Philippe, J. J., Mercker, E. and Preisser, J. S., "HHC Aeroacoustic Rotor Test at the DNW," The Joint German / French / US Project, 20th European Rotorcraft Forum, Amsterdam, 1994.

44. Splettstoesser, W. R., Kube, R., Seelhorst, U., Wagner, W., Boutier, A., Micheli, F., Mercker, E., Pengel, K., "Key Results From a Higher Harmonic Control Aeroacoustic Rotor Test (HART) in the German-Dutch Wind Tunnel," 21st European Rotorcraft Forum, Saint-Petersburg, Russia, 1995.

45. Kube, R., Splettstoesser, W. R., Wagner, W., Seelhorst, U., Yu, Y. H., Boutier, A., Micheli, F. and Mercker, W., "Initial Results From the Higher Harmonic Control Aeroacoustic Rotor Test (HART) in the German-Dutch Wind Tunnel," 75th Fluid Dynamics Panel Symposium on Aerodynamics and Aeroacoustics of Rotorcraft, Berlin, October 10-13, 1994.

46. Brooks, T. F., "The Effect of Signal Jitter on the Spectrum of Rotor Impulsive Noise," *Vertica*, vol. 12, no. 3, 1988, pp. 257-265.

47. Howe, M.S., "A Review of the Theory of Trailing Edge Noise," *Journal of Sound and Vibration*, vol. 61, pp.437-465, 1978.

48. Amiet, R.K., "A Note on Edge Noise Theories," *Journal of Sound and Vibration*, vol. 78, no. 4, pp.485-488, 1981.

49. Goldstein, M.E., "Scattering and Distortion of the Unsteady Motion on Transversely Sheared Mean Flows," *Journal of Fluid Mechanics*, vol. 91, pp.602-632, 1971.

50. Dowling, A.P. and Williams, J.E.F., *Sound and Sources of Sound*, Ellis Horwood Limited, West Sussex, England, 1983.

51. Abbott, I.H. and Doenhoff, A.E.von, *Theory of Wing Sections – Including a Summary of Airfoil Data*, Dover Pub. Inc, New York, 1949.

52. Schlichting, H., *Boundary-Layer Theory*, McGraw-Hill Book Co., New York, 1955.